

A Computer Modeling Study of Defect and Dopant States in SnO₂

C. M. FREEMAN

*Department of Chemistry, University of Keele,
Staffs ST5 5BG, United Kingdom*

AND C. R. A. CATLOW

*Davy Faraday Research Laboratory, Royal Institution,
21 Albemarle Street, London W1X 4BS, United Kingdom*

Received February 6, 1989; in revised form October 4, 1989

We present results of a computer modeling study of the technologically important material SnO₂. We concentrate on the properties of defects and dopants and show first that vacancy energies are high, leading to limited deviations from stoichiometry. Second, we find that both vacancy and interstitial (self-compensating) modes of solution may have low energies for low valence dopants. Oxidation of *p*-type doped material is found to be endothermic, hence poor conductivity is expected. In contrast we calculate that *n*-type doped samples can be exothermically reduced, and would consequently predict high conductivity for such materials. © 1990 Academic Press, Inc.

I. Introduction

The technologically important properties of ionic semiconductors such as SnO₂ are largely determined by the underlying defect chemistry of the material. Indeed in technological materials, SnO₂ is deliberately doped to promote desired electrical characteristics (see, for example, Ref. (1)). However, although the central role of such doping strategies in the manufacture of device materials emphasizes their importance, the detailed influence of dopant ions on the electronic properties of the material is often unknown.

SnO₂ is an extrinsic, *n*-type semiconductor which finds uses in devices such as photovoltaic cells and gas sensors. The electrical and physical properties of the material have been thoroughly characterized (see, for example, Refs. (2-5)). However, there

is little information on the detailed atomic nature of lattice defects and impurity states which determine these macroscopic properties. Indeed the dominant point defect responsible for the accommodation of non-stoichiometry in SnO₂ has yet to be unequivocally resolved (3, 6).

It is therefore clear that a thorough investigation of the defect and dopant states of SnO₂ is needed, especially if we are to understand the sensing properties of the material. In this paper we report the application of established computer modeling techniques to the study of intrinsic disorder, electronic states, and impurity ions in SnO₂. Wherever possible we compare our findings with those of previously reported experimental studies. In the following section we describe the simulation methods upon which our study is based and provide details of their application to SnO₂. In Sec-

tion 3 we present the results of the computer modeling of intrinsic disorder in SnO_2 . Section 4 presents results of the application of simulation techniques to the study of dopant ions within the material.

2. Method

The calculations on perfect lattices and defects embedded in the lattice described in this paper are based on the Born model of the ionic solid, in which the crystal is considered to be composed of discrete ions with integral charges. In addition to ionic (coulombic) forces there are "short range" interactions modeled by pairwise potentials of the Born Mayer, or Buckingham form. The model includes the effects of ionic polarization via the incorporation of the "shell" model of Dick and Overhauser (7).

The techniques which permit the application of the Born model outlined above to the investigation of many phenomena in polar solids have gained wide success (see, for example, Refs. (8, 9)). Here we shall briefly describe the modeling of perfect lattices (of importance in deriving potentials) and the modeling of defect states within the lattice. Detailed accounts of the procedures used can be found in Catlow and Mackrodt (10).

2.1. Lattice Potential for SnO_2

The model of SnO_2 used in the present study comprises short range interionic interaction potential terms and shell model intraionic parameters. A given set of such potential parameters permits the calculation of equilibrium structures and a range of crystal properties (see, for example, Ref. (11)). Derivation of suitable potential parameters is achieved via a least-squares fitting procedure where terms in the potential model are iteratively adjusted to yield optimum agreement with experimentally derived crystal properties. The data used in

the present fitting for SnO_2 included unit cell dimensions, unit cell coordinates, static and high frequency dielectric constants, and elastic constants. It was found that the most effective improvement on an existing model for SnO_2 of James (12) was achieved by refining the oxygen-oxygen interaction parameters. The oxygen-oxygen parameters obtained are somewhat different from those used in several previous studies (see Refs. (12-15)). However, at equilibrium separations the noncoulombic interaction between oxygens is very small. Hence calculated properties are comparatively insensitive to this component of the potential model for the solid. For example, when applied to FeO, the oxygen-oxygen potential of this study yields calculated properties in close agreement with an earlier potential (see Ref. (16)). The least-squares refinement of the oxygen-oxygen potential for SnO_2 therefore represents "fine tuning" for this particular structure.

We note that the potential used in the present work to describe the Sn-oxygen interaction is of the Born-Mayer form (i.e., the attractive r^{-6} term is neglected). At lattice spacings the contribution of this term will be comparatively small and its effect should to some extent be incorporated in the Born-Mayer parameters during the least-squares fitting procedure. The potentials used in the calculation of dopant-host interactions (Section 4) are also of this type (see Ref. (14)).

The final set of potential parameters are presented in Table I and calculated crystal properties for this model are collected in Table II along with experimental values for comparison. We should emphasize that the calculated crystal properties are reported for a structure which has been entirely equilibrated by energy minimization. From Table II it is clear that excellent agreement is possible between theory and experiment within the constraints of a wholly ionic model for this solid.

TABLE I
POTENTIAL MODEL FOR SnO₂

Cation	charge ($ e $)	4.0	Shell charge	1.58
			Spring constant	2037.8
			(eV/Å ²)	
Anion	charge ($ e $)	-2.0	Shell charge	-2.47
			Spring constant	23.09
			(eV/Å ²)	
Short-range parameters				
$V(r) = A \exp(-r/\rho) - C/r^6$				
	Interaction	A/eV	$\rho/\text{Å}$	C/eVÅ ⁶
	Sn ⁴⁺ . . . O ²⁻	1056.8	0.3683	0.0
	O ²⁻ . . . O ²⁻	15123.6	0.2230	28.43

Note. Short-range interactions were "cut off", i.e., set to zero for distances greater than $1.5a$ (a = lattice parameter).

2.2. Point Defect Simulations

The methods used to model defect centers in the crystal are based on the approach of Mott and Littleton (17). Here ionic relaxations close to a defect are explicitly allowed while defect interactions with more distant regions of the crystal are determined by an approximate procedure using the macroscopic dielectric properties of the material. This "two region" Mott-Littleton procedure forms the basis of the CASCADE computer program (18) used in the present work. The inner region (region I) used in the calculations contained at least 100 atoms.

It is generally accepted that the accuracy of such defect calculations is determined by the interatomic potentials which describe interactions between lattice ions, and between lattice and defect species (19, 20). As we have seen in the previous section a lattice potential is available which provides a good description of the SnO₂ lattice. It is reasonable, therefore, to extend the use of this model to an investigation of defect states within the material.

We should note that the calculations on

defect states described in the following sections were performed using the equilibrated unit cell and unit-cell dimensions reported in Table II. Thus there are no residual strains due to the nondefective crystal in the explicitly modeled region of the defect simulations.

The calculations were performed on a FPS 164 array processor supported by the NAS 7000 mainframe host computer at the SERC Daresbury Laboratory, UK.

3. Results: Disorder in SnO₂

In this section we report the results of our static simulation calculations on intrinsic disorder and electronic states in SnO₂. The following section describes calculations on the doped material.

TABLE II
CALCULATED AND EXPERIMENTAL CRYSTAL PROPERTIES FOR SnO₂

	Measured	Calculated
Dielectric constants ^a		
Static field		
$\perp c^b$	14.0	13.8
$\parallel c$	9.86	12.5
High frequency		
$\perp c$	3.785	3.894
$\parallel c$	4.175	4.019
Elastic constants ^c		
C_{11} (dyne cm ⁻² × 10 ¹¹)	26.2	29.9
C_{33}	45.0	52.2
C_{44}	10.3	11.1
C_{66}	20.7	22.8
C_{12}	17.7	21.2
C_{13}	15.6	19.8
Structure		
a, b (Å) ^d	4.738	4.706
c / Å	3.186	3.332
Rutile structural parameter, u /lattice units	0.3071	0.3034

^a Ref. (31).

^b $\perp c$ perpendicular to the c axis, $\parallel c$ parallel to the c axis.

^c Ref. (5).

^d Ref. (32).

TABLE III
POINT DEFECT ENERGIES IN SnO₂

a. Isolated defect energies		
Defect	Energy (eV)	Coordinates
O ²⁻ interstitial	-8.31	(<i>u</i> , - <i>u</i> , 0)
Sn ⁴⁺ interstitial	-68.23	(0, $\frac{1}{2}$, 0)
O ²⁻ vacancy	19.39	(<i>u</i> , <i>u</i> , 0)
Sn ⁴⁺ vacancy	87.48	(0, 0, 0)
b. Frenkel and Schottky energies		
Defect	Formation energy per defect (eV)	
Schottky trio	5.19	
Anion Frenkel pair	5.54	
Cation Frenkel pair	9.63	
"Anti" Schottky trio	8.61	

Note. Lattice energy is -110.68 eV. *u* is the rutile structural parameter.

3.1. Intrinsic Disorder in SnO₂

Calculated energies for oxygen and tin interstitials and vacancies are presented in Table III. Interestingly we find that the lowest energy site for an anion interstitial has the coordinates (*u*, -*u*, 0) (*u* being the variable parameter of the rutile structure) and not as might have been expected (0, 0.5, 0) (the center of an unoccupied oxygen octahedron). Combining these defect formation energies with the calculated lattice energy of SnO₂ permits the determination of Frenkel pair and Schottky trio energies; these are reported in Table IIIb. It is clear from these predicted defect formation energies that the predominant mode of intrinsic disorder is of the Schottky type. Vacancy disorder would therefore be expected to be of particular importance in the nonstoichiometric material. Since SnO₂ becomes nonstoichiometric through the loss of oxygen, anion vacancies rather than cation interstitials are predicted to predominate in the reduced material. This prediction accords well with the experimental findings of Samson and Fonstad (4) based on conduc-

tivity measurements on single crystals and the thermogravimetric studies of Koinuma *et al.* (6). In contrast, the electrical conductivity studies on pellets pressed from powders of both Paria and Maiti (3) and Uematsu *et al.* (21) led to conclusions which cast doubt on the anion vacancy model. However, we note that the latter studies were directed toward the characterization of the electrical properties of doped materials with secondary emphasis on the pure material. The former studies (favoring anion vacancies) were primarily concerned with the study of native defects in the pure material.

The intrinsic defect energy for Schottky disorder reported in Table IIIb is comparatively high (~2.5 eV higher than for the isostructural TiO₂; Ref. (15)). Examination of the relaxed atomic positions in the explicitly modeled region of the defect simulations reveals that larger anion displacements are calculated around oxygen vacancies in TiO₂ than in SnO₂. It is the possibility of large anion relaxations which leads to the readier formation of oxygen vacancies within the TiO₂ lattice. TiO_{2-x} can,

of course, accommodate high degrees of nonstoichiometry by the formation of crystallographic shear planes. Shear planes are not, however, observed in SnO₂. Catlow and James (22), using computer simulation techniques, were able to rationalize this observation in terms of the large cation displacement polarizability in TiO₂: cation relaxation in the vicinity of shear planes was sufficiently large to stabilize this form of reduction. The present study reveals that the anion sublattice is able to relax around defects to a greater extent in TiO₂ than in the isostructural SnO₂. Hence we would not expect such large departures from ideal stoichiometry for SnO₂ as are observed in TiO₂—a point which will be amplified below.

3.2. Electron Hole Formation

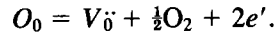
The valence band of SnO₂ is constructed from oxygen 2*p* states and the conduction band from Sn *s*-like orbitals (23). It is thus possible to estimate the band gap of SnO₂ assuming that electron transfer between oxygen and tin ions occurs. Our model for the hole state is thus the localized O⁻ ion while for the electron state it is the Sn³⁺ species. This localized description is probably acceptable for the electron state but is somewhat more questionable for the hole state. Within such a description, however, it is possible to combine CASCADE interatomic energies with free ion intraatomic energy terms to yield formation energies for both states. Here we make the simplifying assumption that such ionization energies differ little from free atom values (see, for example, Ref. (24)). Terms for this band gap computation are collected in Table IV. This calculated value of 4.69 eV for the thermal band gap compares with the experimentally found optical gap of 3.6 (25); the experimental thermal gap will be lower than this value. However, with a band gap of this size SnO₂ will be a poorly conducting material unless its electronic structure is

TABLE IV
ELECTRON-HOLE FORMATION

CASCADE calculated terms	Energy (eV)
$Sn_{sn}' (= e')$	37.84
$O_{\circ} (= h')$	16.33
Intraatomic terms	Energy (eV)
$O^- + e^- \rightarrow O^{2-}$	8.75
$Sn^{3+} \rightarrow e^- + Sn^{4+}$	40.73

Note. The thermal band gap is, therefore, $E_g = 37.84 + 16.33 - 8.75 - 40.73 = 4.69$ eV.

suitably modified. Hence it is found experimentally that high electrical conductivities are only observed in reduced or doped specimens (see, for example, Ref. (26)). In the light of our study of intrinsic disorder in the material (Section 3.1) and previous experimental observations it seems that reduction (or in some cases doping—see Section 4) leads to the formation of doubly ionized oxygen vacancies:



Using our calculated energies we are now in a position to estimate the energetics of this reduction process, E_{RED} , which we may write as

$$E_{RED} = O_{VAC}^{2-} - \frac{1}{2}D_{(O_2)} - E_0 + 2E_e,$$

where O_{VAC}^{2-} is the oxygen vacancy formation energy, $D_{(O_2)}$ the oxygen molecule dissociation energy (for which we use a value of 5.18 eV), and E_0 is the sum of the first and second electron affinities of oxygen; E_e is the energy of introducing an electron into the conduction band of SnO₂ from the vacuum. We calculate a value of 3.65 eV for E_{RED} . Owing to the several approximations involved in the calculation we must be cautious in giving detailed interpretations. But the high positive value suggests only a small deviation from stoichiometry in agreement with experiment.

4. Dopant Ion Calculations

In this section we report calculated energies for dopant ions in the SnO_2 lattice. Such studies need satisfactory potentials for the interaction of dopant ions with the host lattice. For a number of ions, where alternative methods are not available, we have obtained these potentials using electron gas (27) or "shifted electron gas" (28) methods of derivation. However, following Lewis and Catlow (14) we have preferred where possible to use empirically derived potential parameters, fitted to the structural and crystal properties of the dopant oxide in question. We frequently require the calculated lattice energy of the dopant oxide in studies of solution enthalpies and it is important that the dopant oxygen potential be capable of accurately modeling the solute dopant oxide crystal. Appendix I gives details of the potentials used in our calculations.

4.1. Incorporation of Dopants into the SnO_2 Lattice

Defect formation energies have been calculated for a range of cations in the SnO_2 lattice as both substitutional and interstitial modifications of the perfect crystal. These energies are presented in Table V. Solution enthalpies for dopant oxides in SnO_2 may be readily predicted from the calculated lattice energies (Table VI) and appropriate charge compensating defect energies (Table III).

The choice of charge compensating defect is obviously critical in these calculations. We recall that the intrinsic form of disorder predominant in SnO_2 is of the Schottky type and we might therefore expect anion and cation vacancies, respectively, to compensate for negative and positive residual charge upon impurity incorporation. However, we note that experimental studies do not unanimously concur in this expectation (see, for example, Ref. (3)) and we have, therefore, also

reported values for anion and cation interstitial compensation. It is of interest to compare the relative enthalpies of substitutional and interstitial modes of solution. Calculated solution enthalpies are reported in Table VII. (Details of the energy cycles used to prepare this table are given in Appendix 2.) We note that at this stage it has

TABLE V
DEFECT ENERGIES FOR DOPANT IONS IN SnO_2

Cation	Substitutional defect Energy (eV)	Interstitial defect Energy (eV)
Li^+	75.81	-4.97
Na^+	78.26	0.61
K^+	81.73	6.86
Rb^+	83.69	9.96
Mg^{2+}	55.30	-20.72
Ca^{2+}	60.26	-12.37
Sr^{2+}	63.67	-7.23
Mn^{2+}	57.35	-17.41
Fe^{2+}	56.14	-19.35
Co^{2+}	55.57	-20.16
Ni^{2+}	55.03	-21.15
Ba^{2+}	62.14	-9.26
Al^{3+}	25.22	-49.11
Sc^{3+}	30.78	-40.56
Ti^{3+}	28.16	-44.17
V^{3+}	28.41	-43.70
Cr^{3+}	34.57	-34.92
Mn^{3+}	28.19	-44.65
Fe^{3+}	28.62	-44.23
Y^{3+}	35.51	-33.44
Ce^{3+}	41.62	-24.52
Nd^{3+}	38.66	-28.91
Er^{3+}	37.27	-30.89
Gd^{3+}	36.93	-31.40
Ho^{3+}	35.46	-33.50
Yb^{3+}	34.44	-35.04
Lu^{3+}	34.02	-35.61
Pu^{3+}	38.41	-29.26
Ti^{4+}	-1.18	-70.80
Si^{4+}	-12.31	-85.33
Pb^{4+}	8.60	-55.56
Mn^{4+}	-2.74	-71.29
Zr^{4+}	2.92	-63.39
Ce^{4+}	7.59	-56.95
U^{4+}	12.02	-51.33
Th^{4+}	12.22	-51.12

TABLE VI
LATTICE ENERGIES OF DOPANT
OXIDES

Oxide	Lattice energy (eV)
Li ₂ O	-29.98
Na ₂ O	-24.75
K ₂ O	-22.18
Rb ₂ O	-21.18
MgO	-41.29
CaO	-35.95
SrO	-33.42
MnO	-38.73
FeO	-40.12
CoO	-40.83
NiO	-41.58
BaO	-33.74
Al ₂ O ₃	-160.50
Sc ₂ O ₃	-144.47
Ti ₂ O ₃	-150.36
V ₂ O ₃	-150.37
Cr ₂ O ₃	-136.82
Mn ₂ O ₃	-150.82
Fe ₂ O ₃	-150.85
Y ₂ O ₃	-134.74
Ce ₂ O ₃	-124.36
Nd ₂ O ₃	-129.22
Eu ₂ O ₃	-131.56
Gd ₂ O ₃	-132.16
Ho ₂ O ₃	-134.79
Yb ₂ O ₃	-136.76
Lu ₂ O ₃	-137.55
Pu ₂ O ₃	-129.63
TiO ₂	-112.45
SiO ₂	-126.12
PbO ₂	-103.44
MnO ₂	-113.77
ZrO ₂	-108.25
CeO ₂	-104.26
UO ₂	-100.59
ThO ₂	-100.38

Note. Taken from Lewis (13).

not been possible to derive potentials that adequately model Sb₂O₅ which is an important dopant. We can, however, make important general conclusions about the mode of solution of pentavalent dopants, for which our calculated defect energies strongly favor compensation by cation vacancies.

From the solution enthalpies presented in Table VII it is clear that tetravalent dopants show a strong preference for substitutional solution in SnO₂. However, for mono-, di-, and trivalent dopants two forms of solution are important. For the lighter elements "self charge-compensation" is energetically favored leading to the formation of both substitutional and interstitial dopant ions within the lattice. The heavier elements form substitutional solutions with anion vacancy charge compensation. Which of these two modes of solution predominates will clearly have an important bearing on the properties of doped SnO₂. However, we note that at present our model takes no account of the possible interaction of the dopant cation with a charge-compensating defect.

For the "light" mono-, di-, and trivalent cation impurity ions in SnO₂ (those favoring "self-compensation") there will be a proportion of dopant species in interstitial sites. We recall that the interstitial site in SnO₂ is in the vacant channel within the rutile structure. Analogy with previous experimental studies on TiO₂ (see, for example, Refs. (29, 30)) and theoretical studies currently underway on SnO₂ indicate that ionic migration occurs readily along this channel. Thus we would expect impurity migration to be strongly facilitated in doped samples—a direct result of the "self-compensating" mode of solution experienced by these ions. This finding will be of importance in the understanding of device aging characteristics which may proceed via dopant migration. For the tri- and tetravalent dopants predicted to form substitutional solutions with oxygen vacancy compensation, impurity migration would be considerably slower.

5. Redox Properties of Doped SnO₂

One of the main objectives of doping SnO₂ is to modify its electrical properties.

TABLE VII
ENERGIES OF SOLUTION FOR OXIDES IN SnO₂

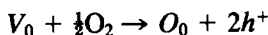
Oxide	Mode of solution				
	Substitutional dopant anion vacancy compensation	Substitutional dopant cation interstitial compensation	Interstitial dopant anion interstitial compensation	Interstitial dopant cation vacancy compensation	Substitutional interstitial dopant compensation
Li ₂ O	9.20	11.96	5.87	4.22	2.55
Na ₂ O	9.04	11.79	8.83	7.19	4.73
K ₂ O	11.22	13.98	13.79	12.15	9.00
Rb ₂ O	12.69	15.44	16.39	14.75	11.31
MgO	5.30	7.14	12.26	8.97	3.24
CaO	4.92	6.76	15.27	11.98	4.56
SrO	5.80	7.64	17.88	14.59	6.30
MnO	4.79	6.63	13.01	9.72	3.36
FeO	4.97	6.81	12.46	9.17	3.18
CoO	5.16	6.95	12.36	9.07	2.49
NiO	5.32	7.16	12.12	8.83	3.18
BaO	4.59	6.43	16.17	12.88	4.84
Al ₂ O ₃	4.49	5.40	18.68	13.74	3.88
Sc ₂ O ₃	2.03	2.95	19.21	14.28	2.17
Ti ₂ O ₃	2.36	3.27	18.55	13.61	2.25
V ₂ O ₃	2.61	3.53	19.02	14.09	2.56
Cr ₂ O ₃	1.99	2.91	21.03	16.09	2.60
Mn ₂ O ₃	2.62	3.53	18.30	13.36	2.38
Fe ₂ O ₃	3.06	3.98	18.75	13.80	2.82
Y ₂ O ₃	1.90	2.81	21.47	16.53	2.63
Ce ₂ O ₃	2.82	3.73	25.20	20.26	4.26
Nd ₂ O ₃	2.29	3.20	23.24	18.30	3.37
Eu ₂ O ₃	2.07	2.98	22.43	17.49	3.00
Gd ₂ O ₃	2.03	2.94	22.22	17.28	2.92
Ho ₂ O ₃	1.87	2.79	21.43	16.50	2.61
Yb ₂ O ₃	1.84	2.75	20.88	15.94	2.44
Lu ₂ O ₃	1.81	2.73	20.70	15.77	2.38
Pu ₂ O ₃	2.24	3.16	23.09	18.16	3.30
TiO ₂	0.59 ^a	—	25.03	18.45	—
SiO ₂	3.13 ^a	—	24.17	17.59	—
PbO ₂	1.36 ^a	—	31.26	24.68	—
MnO ₂	0.35 ^a	—	25.86	19.28	—
ZrO ₂	0.49 ^a	—	28.24	21.66	—
CeO ₂	1.17 ^a	—	30.69	24.11	—
UO ₂	1.93 ^a	—	32.64	26.06	—
ThO ₂	1.92 ^a	—	32.64	26.06	—

^a No charge compensating defect is necessary for the tetravalent impurities in substitutional sites (see Appendix 2).

Hole states will be created on oxidation of materials doped with low valence ions (provided that these are not self-compensating

as discussed in the previous section), and electron states, by reduction of high valent (penta- or hexavalent ion) doped materials.

In the former case the defect reaction will be

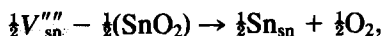


for which we can write the energy expression

$$E_{ox} = -O_{VAC}^2 + \frac{1}{2}D_{(O_2)} + E_0 + 2E_h,$$

where E_h is the energy to create a hole by removing an electron to the vacuum. Using the energies previously calculated or quoted we obtain an energy of 5.53 eV. This high value indicates that good p -type conductivity will require very high oxygen pressures. The difficulty in producing good p -type conduction in SnO₂ will be enhanced by the tendency for self-compensation of at least the lighter low valence dopants.

Very different behavior is found with the pentavalent dopants, for which the appropriate redox reaction is



where by (SnO₂) we indicate a mole of SnO₂ (from the surface) which is consumed in the reduction process. The energy of this reaction, E_{RED} , may be written as

$$E_{RED} = \frac{1}{2}Sn_{VAC}^{4+} - \frac{1}{2}E_L^{SnO_2} - \frac{1}{2}D_{(O_2)} - \frac{1}{2}E_0,$$

where Sn_{VAC}^{4+} is the formation energy of the tin vacancy and $E_L^{SnO_2}$ is the lattice energy of SnO₂. The calculated value of E_{RED} is -1.53 eV. This favorable energy indicates that reduction is a thermodynamically favorable process in, e.g., Sb(v) doped materials and that as a consequence pentavalent doped materials will be good n -type semiconductors.

6. Conclusions and Future Work

The work described in this report has dealt with the problems of intrinsic disorder and dopant oxide solution in SnO₂. Three main conclusions are evident from this

study. First, we find that in the nonstoichiometric SnO_{2-x}, anion vacancies will be the dominant type of defect. In this context, further work in which mass action techniques are employed to study interaction of bulk SnO₂ with its gaseous environment is planned. Second, in the doped material, for many important impurity ions, a significant proportion of dopant species will be in interstitial sites. This self-compensating mode of solution will facilitate dopant ion migration. Third, we predict that while doping with trivalent ions leads to only poor p -type behavior, doping with pentavalent species will result in good n -type conductivity.

There remain several problems in the study of SnO₂ which the present report has not addressed. The energetics of dopant ion-defect interactions may be determined with the Mott-Littleton approach, as may the migration energy as for ionic materials. The results of such calculations will be reported in the future.

Appendix 1

Potential Parameters Used in Defect Calculations

Interaction	A(eV)	ρ (Å)	Method of derivation
Li ⁺ -O ²⁻	292.3	0.3472	e.g.
Na ⁺ -O ²⁻	611.1	0.3535	e.g.
K ⁺ -O ²⁻	902.8	0.3698	e.g.
Rb ⁺ -O ²⁻	1010.8	0.3793	e.g.
Mg ²⁺ -O ²⁻	1428.5	0.2945	e.g.
Ca ²⁺ -O ²⁻	1090.4	0.3437	em.
Sr ²⁺ -O ²⁻	959.1	0.3721	em.
Mn ²⁺ -O ²⁻	1007.4	0.3262	em.
Fe ²⁺ -O ²⁻	1207.6	0.3084	em.
Co ²⁺ -O ²⁻	1491.7	0.2951	em.
Ni ²⁺ -O ²⁻	1582.5	0.2882	em.
Ba ²⁺ -O ²⁻	1214.4	0.3522	em.
Al ³⁺ -O ²⁻	1474.4	0.3006	em.
Sc ³⁺ -O ²⁻	1299.4	0.3312	em.
Ti ³⁺ -O ²⁻	1715.7	0.3069	em.
V ³⁺ -O ²⁻	1790.2	0.3061	em.
Cr ³⁺ -O ²⁻	1255.2	0.3490	e.g.

Appendix 1

Interaction	A(eV)	$\rho(\text{\AA})$	Method of derivation
Mn ³⁺ -O ²⁻	1257.9	0.3214	em.
Fe ³⁺ -O ²⁻	1102.4	0.3299	em.
Y ³⁺ -O ²⁻	1345.1	0.3491	em.
Ce ³⁺ -O ²⁻	1732.2	0.3588	e.g.
Nd ³⁺ -O ²⁻	1379.9	0.3601	em.
Er ³⁺ -O ²⁻	1358.0	0.3556	em.
Gd ³⁺ -O ²⁻	1336.8	0.3551	em.
Ho ³⁺ -O ²⁻	1350.2	0.3487	em.
Yb ³⁺ -O ²⁻	1309.6	0.3462	em.
La ³⁺ -O ²⁻	1347.1	0.3430	em.
Pu ³⁺ -O ²⁻	1376.2	0.3593	em.
Sn ³⁺ -O ²⁻	858.4	0.3849	s.e.g.
Ti ⁴⁺ -O ²⁻	754.2	0.3879	em.
Si ⁴⁺ -O ²⁻	913.2	0.3428	e.g.
Pb ⁴⁺ -O ²⁻	2168.4	0.3489	e.g.
Mn ⁴⁺ -O ²⁻	1396.4	0.3440	e.g.
Zr ⁴⁺ -O ²⁻	1608.1	0.3509	e.g.
Ce ⁴⁺ -O ²⁻	1986.8	0.3511	e.g.
U ⁴⁺ -O ²⁻	2246.8	0.3554	e.g.
Th ⁴⁺ -O ²⁻	2201.1	0.3570	e.g.
Sn ²⁺ -O ²⁻	638.5	0.4079	s.e.g.

Abbreviations used: em., empirical (13); e.g., electron gas (27); s.e.g., shifted electron gas (28).

Appendix 2

Calculation of Solution Enthalpies for Dopant Oxides

A. Monovalent Oxide, M₂O

(a) Substitutional solution, anion vacancy compensation

$$E_{S_1} = M_{\text{subs}}^+ + \frac{3}{2}O_{\text{vac}}^{2-} + E_L^{\text{SnO}_2} - \frac{1}{2}E_L^{M_2O}$$

(b) Substitutional solution, cation interstitial compensation

$$E_{S_2} = M_{\text{subs}}^+ + \frac{3}{4}Sn_{\text{int}}^{4+} + \frac{1}{4}E_L^{\text{SnO}_2} - \frac{1}{2}E_L^{M_2O}$$

(c) Interstitial solution, anion interstitial compensation

$$E_{I_1} = M_{\text{int}}^+ + \frac{1}{2}O_{\text{int}}^{2-} - \frac{1}{2}E_L^{M_2O}$$

(d) Interstitial solution, cation vacancy compensation

$$E_{I_2} = M_{\text{int}}^+ + \frac{1}{4}Sn_{\text{vac}}^{4+} + \frac{1}{4}E_L^{\text{SnO}_2} - E_L^{M_2O}$$

(e) Self-compensation

$$E_{\text{self}} = \frac{1}{4}M_{\text{subs}}^+ + \frac{3}{4}M_{\text{int}}^+ + \frac{1}{4}E_L^{\text{SnO}_2} - \frac{1}{2}E_L^{M_2O}$$

Key

M_{subs}^+ : Energy to replace Sn⁴⁺ at lattice site by M⁺.

M_{int}^+ : Energy to introduce M⁺ into interstitial site.

O_{vac}^{2-} : Energy to create oxygen vacancy.

O_{int}^{2-} : Energy to introduce oxygen interstitial.

Sn_{vac}^{4+} : Energy to create tin vacancy.

Sn_{int}^{4+} : Energy to introduce Sn⁴⁺ interstitial.

$E_L^{\text{SnO}_2}$: Lattice energy of SnO₂.

$E_L^{M_2O}$: Lattice energy of M₂O.

B. Divalent Oxide, MO

(a) Substitutional solution, anion vacancy compensation

$$E_{S_1} = M_{\text{subs}}^{2+} + O_{\text{vac}}^{2-} + E_L^{\text{SnO}_2} - E_L^{MO}$$

(b) Substitutional solution, cation interstitial compensation

$$E_{S_2} = M_{\text{subs}}^{2+} + \frac{1}{2}Sn_{\text{int}}^{4+} + \frac{1}{2}E_L^{\text{SnO}_2} - E_L^{MO}$$

(c) Interstitial solution, anion interstitial compensation

$$E_{I_1} = M_{\text{int}}^{2+} + O_{\text{int}}^{2-} - E_L^{MO}$$

(d) Interstitial solution, cation vacancy compensation

$$E_{I_2} = M_{\text{int}}^{2+} - \frac{1}{2}Sn_{\text{vac}}^{4+} + \frac{1}{2}E_L^{\text{SnO}_2} - E_L^{MO}$$

(e) Self-compensation

$$E_{\text{self}} = \frac{1}{2}M_{\text{subs}}^{2+} + \frac{1}{2}M_{\text{int}}^{2+} + \frac{1}{2}E_L^{\text{SnO}_2} - E_L^{MO}$$

Key

As above plus E_L^{MO} : Lattice energy of MO.

C. Trivalent Oxide, M₂O₃

(a) Substitutional solution, anion vacancy compensation

$$E_{S_1} = M_{\text{subs}}^{3+} + \frac{1}{2}O_{\text{vac}}^{2-} + E_L^{\text{SnO}_2} - \frac{1}{2}E_L^{M_2O_3}$$

(b) Substitutional solution, cation interstitial compensation

$$E_{S_2} = M_{\text{subs}}^{3+} + \frac{1}{4}Sn_{\text{int}}^{4+} + \frac{3}{4}E_L^{\text{SnO}_2} - \frac{1}{2}E_L^{M_2O_3}$$

(c) Interstitial solution, anion interstitial compensation

$$E_{I_2} = M_{\text{int}}^{3+} + \frac{3}{4}Sn_{\text{vac}}^{4+} + \frac{3}{4}E_L^{\text{SnO}_2} - \frac{1}{2}E_L^{M_2O_3}$$

(d) Interstitial solution, cation vacancy compensation

$$E_{I_2} = M_{\text{int}}^{3+} + \frac{3}{4}O_{\text{int}}^{2-} + \frac{3}{4}E_L^{\text{SnO}_2} - \frac{1}{2}E_L^{M_2O_3}$$

(e) Self-compensation

$$E_{\text{self}} = \frac{3}{4}M_{\text{sub}}^{3+} + \frac{1}{4}M_{\text{int}}^{3+} + \frac{3}{4}E_L^{\text{SnO}_2} - \frac{1}{2}E_L^{M_2O_3}$$

Key

As above plus $E_L^{M_2O_3}$: Lattice energy of M_2O_3 .

D. Tetravalent Oxide, MO₂

(a, b, e) substitutional solution

$$E_{S_1} = E_{S_2} = E_{\text{self}} = M_{\text{subs}}^{4+} + E_L^{\text{SnO}_2} - E_L^{MO_2}$$

(c) interstitial solution, anion interstitial compensation

$$E_{I_1} = M_{\text{int}}^{4+} + 2O_{\text{int}}^{2-} - E_L^{MO_2}$$

(d) interstitial solution, cation vacancy compensation

$$E_{I_2} = M_{\text{int}}^{4+} + Sn_{\text{vac}}^{4+} + E_L^{\text{SnO}_2} - E_L^{MO_2}$$

Key

As above plus $E_L^{MO_2}$: Lattice energy of MO₂.

References

1. S. R. MORRISON, *Sens. Actuators* **2**, 329 (1982).
2. J. A. MARLEY AND R. C. DOCKERTY, *Phys. Rev. A* **140**, 304 (1965).
3. M. K. PARIJA AND H. S. MAITI, *J. Mater. Sci.* **18**, 2101 (1983).
4. S. SAMSON AND C. G. FONSTAD, *J. Appl. Phys.* **44**, 4618 (1973).
5. E. CHANG AND E. K. GRAHAM, *J. Geophys. Res.* **80**, 2595 (1975).
6. H. KOINUMA, J. SHIMOYAMA, J. MIZUSAKI, M. KAWASAKI, AND K. FUEKI, *Ext. Abstr. 18th (1986) Int. Conf. Solid State Devices Mater.*, 763 (1986).
7. B. G. DICK AND A. W. OVERHAUSER, *Phys. Rev.* **112**, 90 (1958).
8. C. R. A. CATLOW, *Annu. Rev. Mater. Sci.* **16**, 517 (1986).
9. G. V. LEWIS, C. R. A. CATLOW, AND R. E. W. CASSELTON, *J. Amer. Ceram. Soc.* **68**, 555 (1985).
10. C. R. A. CATLOW AND W. C. MACKRODT, "Computer Simulation of Solids," Springer-Verlag, New York/Berlin (1982).
11. S. C. PARKER, A. N. CORMACK, AND C. R. A. CATLOW, *Acta Crystallogr. B* **40**, 200 (1984).
12. R. JAMES, Ph.D., thesis, University of London, available as UKAEA Report AERE TP, 814 (1979).
13. G. V. LEWIS, Ph.D. University of London (1983).
14. G. V. LEWIS AND C. R. A. CATLOW, *J. Phys. C.* **18**, 1149 (1985).
15. C. R. A. CATLOW, C. M. FREEMAN, AND R. L. ROYLE, *Physica B* **131**, 1 (1985).
16. C. R. A. CATLOW AND B. E. F. FENDER, *J. Phys. C.* **8**, 3267 (1975).
17. N. F. MOTT AND M. J. LITTLETON, *Trans. Faraday Soc.* **34**, 485 (1938).
18. M. LESLIE, Daresbury Laboratory Report, DL/SCI/TM3IT (1982).
19. C. R. A. CATLOW, *J. Phys. C.* **6**, 53 (1980).
20. C. R. A. CATLOW, J. CORISH, K. M. DILLER, P. W. M. JACOBS, AND M. J. NORGETT, *J. Phys. C.* **12**, 451 (1979).
21. K. UEMATSU, N. MIZUTANI, AND M. KATO, *J. Mater. Sci.* **22**, 915 (1987).
22. C. R. A. CATLOW AND R. JAMES, *Proc. R. Soc. London Ser. A* **384**, 157 (1982).
23. J. ROBERTSON, *Phys. Rev. B* **30**, 3520 (1984).
24. C. R. A. CATLOW AND D. G. MUXWORTHY, *Phil. Mag. B* **37**, 63 (1978).
25. J. ROBERTSON, *J. Phys. C.* **12**, 4767 (1979).
26. M. NAGASAWA AND S. SHIONOYA, *Japan. J. Appl. Phys.* **10**, 472 (1971).
27. R. G. GORDON AND Y. S. KIM, *J. Chem. Phys.* **56**, 3122 (1972).
28. A. D. MURRAY, Ph.D. thesis, University of London (1985).
29. J. R. AKSE AND H. B. WHITEHURST, *J. Phys. Chem. Sol.* **39**, 457 (1978).
30. J. SASAKI, N. L. PETERSON, AND K. HOSHINO, *J. Phys. Chem. Sol.* **46**, 1267 (1985).
31. R. SUMMITT, *J. Appl. Phys.* **39**, 3762 (1968).
32. W. H. BAUR AND A. A. KHAN, *Acta Crystallogr. B* **27**, 2133 (1971).